

Impact of Instrument Transformers and Anti-Aliasing Filters on Fault Locators

R. L. A. Reis, W. L. A. Neves, and D. Fernandes Jr.

Abstract—Butterworth and Chebyshev anti-aliasing filters assembled in instrument transformers (IT) affect the signal waveform inputs to relays and consequently the protection performance. Here, investigations were carried out for the following case studies: two-ended travelling wave-based and one- and two-terminal impedance-based fault locators. Two coupling capacitor voltage transformers (CCVT) and one current transformer (CT) available in literature were used. Several fault simulations were performed in the Alternative Transients Program (ATP) and the fault point was estimated considering the primary, secondary, and filtered secondary signals. From the obtained results, the techniques' reliability are directly affected by the IT and filters transient responses.

Keywords: Instrument transformers, travelling waves, impedance-based, fault location, anti-aliasing filters.

I. INTRODUCTION

VOLTAGE and current signals containing information about disturbances in power systems are delivered to protective devices via instrument transformers (IT). The IT, as Coupling Capacitor Voltage Transformers (CCVT) and Current Transformers (CT), are fundamental equipments for protection systems since they provide scaled-down replicas of power network voltage and current signals at fundamental frequency to safe and practical levels to operate with [1], [2].

The conventional CCVT and CT are based on electromagnetic coupling between the electric power system on the primary side and the protective and control devices on the secondary side, providing voltage and current measurements with acceptable accuracy for the most demanding applications. However, due to such design, the IT exhibit undesired transient behavior under fault conditions on power grid in such a way that the secondary voltage and current waveforms are not similar to the primary signals. As a result, malfunctioning in fault location algorithms or substantial delay in the tripping process of protective relays may take place [2]–[4].

Before secondary signals are sampled by analog-to-digital (A/D) converters to be used as input data in numerical relays and fault locators, analog low-pass anti-aliasing filters are applied for both voltage and current signals in order to prevent the occurrence of aliasing phenomenon, which may lead to sinusoidal frequency and phase changing on the sampled

signals if the sampling rate of the A/D converters is less than twice the maximum frequency presented in the secondary signals. Generally, a second or third order Butterworth, Chebyshev or Bessel filters may be used to satisfy computer relaying requirements [1], [3]. Depending on the filter used, distortions on the IT secondary signals during fault situations on the power system may become more evident or attenuated, affecting the fault location techniques' accuracy.

In literature, there are several references indicating the influence of the IT-induced transient behavior on the performance of the protection and fault location algorithms [2], [4], [5]. However, the authors are not aware of references indicating the impact of IT+anti-aliasing filters on the fault location techniques' performances in english literature, subject that still demands more investigations.

With the purpose of investigating in detail the effects of the IT transient behavior on the performance of fault location methods, it is analyzed in this work the impact of two 230 kV CCVT and one CT models obtained from the literature, and three anti-aliasing filters on a two-ended traveling wave-based and one- and two-ended impedance-based fault location routines. Considering the travelling wave-based fault location, the fault-induced transients were detected using a method based on the Maximal Overlap Discrete Wavelet Transform (MODWT) [6]. The evaluations are performed by a great amount of fault simulations on a 230 kV power network using the Alternative Transients Program [7]. In each simulation, the fault location, resistance, type and inception angle are varied. The fault location errors are compared when the following signals are used as input to the fault location algorithms: voltage and current ideal measurements (taken from the power system primary side), secondary measurements (taken from CCVTs and CT), and filtered secondary measurements (taken from CCVTs, CT, and anti-aliasing filters in cascade).

II. FAULT LOCATION ALGORITHMS

In this paper, the performance of travelling wave-based and impedance-based fault locators techniques are evaluated in relation to the impact of different IT models.

A. Travelling Wave-Based Technique

After a fault inception in a power network, voltage and current transients travel along the transmission line (TL) toward both line terminals. These transients continue to travel back and forth between the fault point and line ends until the power system reaches a new post-fault steady-state of operation. The travelling wave-based routines take into account the higher frequency components presented at the voltage and/or current

R. L. A. Reis is with Federal Rural University of Pernambuco, 52.171-011 Cabo de Santo Agostinho, Brazil, and currently he is a PhD student at Federal University of Campina Grande, Campina Grande, Brazil. e-mail: raphael.reis@ufrpe.br.

W. L. A. Neves and D. Fernandes Jr. are with the Department of Electrical Engineering at Federal University of Campina Grande, 58.429-900 Campina Grande, Brazil. (e-mail: waneves, damasio@dee.ufcg.edu.br).

Paper submitted to the International Conference on Power Systems Transients (IPST2017) in Seoul, Republic of Korea June 26-29, 2017

transient waveforms to estimate the fault location [1]. These techniques need high sampling rates to adequately reproduce the higher frequency components presented at voltage and/or current signals. In this paper, the sampling rate used for the travelling wave-based fault locators was chosen as 50 kHz.

The two-terminal methods are reported as more reliable and accurate since they need to detect the first incident waves at the monitored buses only, although the data synchronization between both line ends are required. Here, the two-ended algorithm proposed in [8] is implemented. As the goal of this paper is investigate the impact of IT on fault locators' performances, the communication link between both TL terminals is considered as perfect.

According to [8], the estimated fault point \tilde{d} is computed by:

$$\tilde{d} = \frac{\ell + (t_1 - t_2) \cdot v}{2}, \quad (1)$$

where ℓ is the TL length, t_1 and t_2 are the time instants in which the first travelling waves are detected at the local and remote buses, respectively, and v is the aerial mode travelling wave propagation speed, which was taken as 98% of the light speed, as suggested by [9].

In order to detect the fault-induced transients and estimate the time instants t_1 and t_2 , the method reported in [6] was used, which is based on the spectral energy of the wavelet coefficients. According to [6], during the steady-state, the wavelet coefficients energy magnitude is lower than $\mu + 4\sigma$ (steady-state threshold), where μ and σ are the wavelet coefficients energy magnitude average and standard deviation, respectively. When the power grid is subject to fault conditions, the wavelet coefficients energy present higher magnitudes than the steady-state threshold, allowing the fault-induced transients detection.

B. Impedance-Based Techniques

The impedance-based techniques estimate the fault distance from the apparent impedance computed between the monitored TL bus and the location of the short-circuit. The performance of one- and two-terminal methods are evaluated in this paper. The sampling rate used for these routines was chosen as 960 Hz.

1) *One-Ended Method*: One-ended algorithms are reported as straightforward to implement, yield reasonable location estimates, and do not need any communication channel or data synchronization between local and remote buses [10].

Here, the technique reported in [11] was used, which estimates the fault point \tilde{d} by:

$$\tilde{d} = \frac{\text{imag}(V_G \cdot \Delta I_G^*)}{\text{imag}(Z_{L1} \cdot I_G \cdot \Delta I_G^*)}, \quad (2)$$

where V_G , I_G , and ΔI_G are the voltage, current, and the "pure fault" current phasors taken from the monitored TL end, respectively. These values depend on the fault type. In this paper, the phasor quantities are computed using the full cycle discrete fourier transform applied with a mimic filter for decaying DC offset removal [3], [12].

2) *Two-Ended Method*: Two-terminal methods use voltage and current data captured at both TL ends to estimate the fault point. Measurements taken from the remote bus eliminate any reactance error caused by fault resistance or system non-homogeneity, features that considerable affect one-ended techniques. The data synchronization is considered as perfect in this work.

The fault location \tilde{d} is estimated using [10]:

$$d = \frac{V_{G2} - V_{H2} + Z_{L2} \cdot I_{H2}}{(I_{G2} + I_{H2}) \cdot Z_{L2}}, \quad (3)$$

where V_{G2} and V_{H2} are the negative-sequence voltages at local and remote ends, respectively. I_{G2} and I_{H2} are the negative-sequence currents at local and remote TL ends, respectively, and Z_{L2} is the negative-sequence TL impedance. For three-phase balanced faults, which present just positive-sequence components, (3) may be applied by replacing the negative-sequence components to positive-sequence components [10].

III. THE ANALYZED IT AND ANTI-ALIASING FILTERS

A. Anti-Aliasing Filters

The digital frequency of the set of samples obtained during the sampling process performed by A/D converters is equal to the analog frequency of the continuous signal if the sampling rate (f_s) is at least twice the maximum frequency of the sampled analog signal (f), that is ($f_s = 2f$), which is called Nyquist frequency [1], [3]. Sampling a continuous signal with maximum frequency higher than $f = f_s/2$ results in obtaining digital information with frequency different from that at the input of A/D converters. This phenomenon of changing frequency during the sampling process is called aliasing, which also causes a phase-change effect [1]. In this way, analog low-pass anti-aliasing filters are applied prior to sampling to prevent the aliasing phenomenon occurrence by removing frequencies higher than $f_s/2$.

In most computer relaying applications, a second or third order Butterworth, Chebyshev, or Bessel filters may be used to satisfy numerical relaying requirements [3]. Despite Chebyshev filters present more oscillations along the bandpass, the number of works investigating their impact on fault location and protection procedures are still limited. In this context, the performance of a second and a third order Butterworth and a third order Chebyshev filters are evaluated in this paper in cascade with the IT presented in section III-B for the fault location analysis.

Since the sampling rate for the travelling wave-based fault location algorithm used in this paper is 50 kHz (see section II-A), the cut-off frequency (f_c) of the anti-filters must be at most 25 kHz, according to the Nyquist criteria. Here, as the CCVT 1 presents a frequency response up to 10 kHz (see section III-B), f_c was chosen as 9 kHz. The second order Butterworth transfer function (H_{9B2}), the third order Butterworth transfer function (H_{9B3}), and the third order Chebyshev transfer function (H_{9C3}) are described in (4), (5), and (6), respectively.

$$H_{9B2} = \frac{3.198 \cdot 10^9}{s^2 + 7.997 \cdot 10^4 s + 3.198 \cdot 10^9}, \quad (4)$$

$$H_{9B3} = \frac{1.808 \cdot 10^{14}}{s^3 + 1.131 \cdot 10^5 s^2 + 6.396 \cdot 10^9 s + 1.808 \cdot 10^{14}}, \quad (5)$$

$$H_{9C3} = \frac{4.531 \cdot 10^{13}}{s^3 + 3.377 \cdot 10^4 s^2 + 2.969 \cdot 10^9 s + 4.531 \cdot 10^{13}}. \quad (6)$$

For the impedance-based techniques, since $f_s = 960$ Hz (see section II-B), the anti-aliasing f_c must be, at most, 480 Hz. Here, $f_c = 180$ Hz was used. The second order Butterworth transfer function (H_{180B2}), the third order Butterworth transfer function (H_{180B3}), and the third order Chebyshev transfer function (H_{180C3}) are described in (7), (8), and (9), respectively.

$$H_{180B2} = \frac{1.279 \cdot 10^6}{s^2 + 1599s + 1.279 \cdot 10^6}, \quad (7)$$

$$H_{180B3} = \frac{1.447 \cdot 10^9}{s^3 + 2262s^2 + 2.558 \cdot 10^6 s + 1.447 \cdot 10^9}, \quad (8)$$

$$H_{180C3} = \frac{3.625 \cdot 10^8}{s^3 + 675.5s^2 + 1.187 \cdot 10^6 s + 3.625 \cdot 10^8}. \quad (9)$$

The ideal and anti-aliasing filters frequency responses for $f_c = 180$ Hz and $f_c = 9$ kHz are shown in Fig. 1.

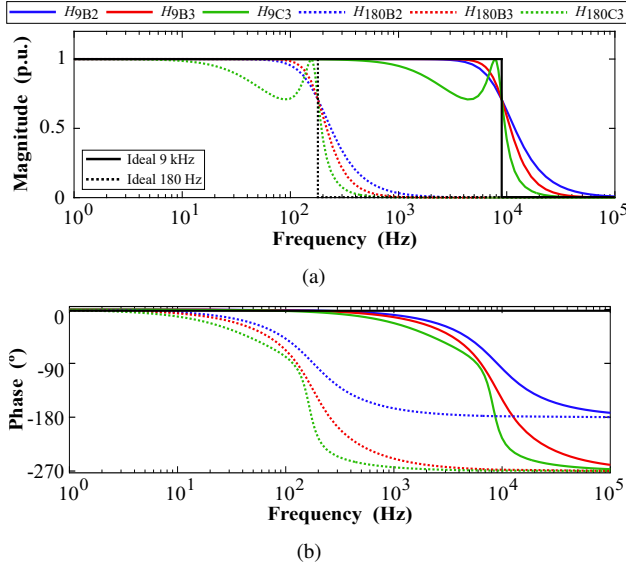


Fig. 1. Ideal, Butterworth, and Chebyshev frequency responses: (a) magnitude; (b) phase.

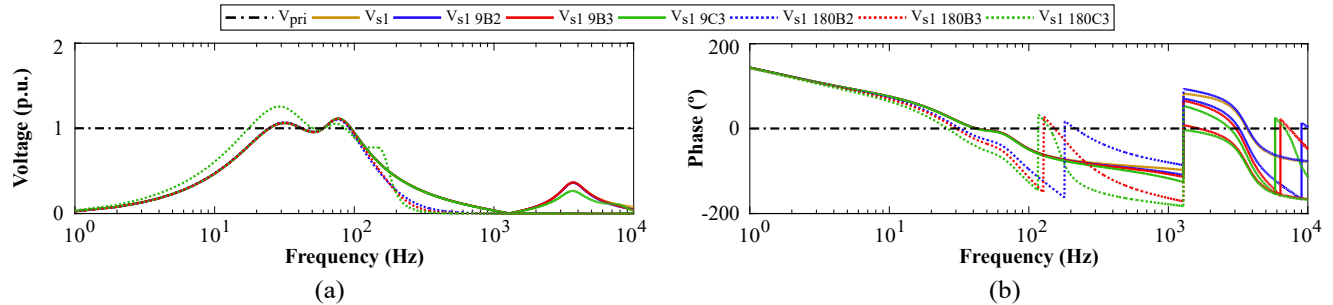


Fig. 2. CCVT 1 frequency response: (a) magnitude (p.u.); (b) phase (°).

B. Analyzed IT

During faults on TL, the IT secondary signals may present transient components not found at the primary waveforms, which may lead to fault locators and relays misoperations [1]. In this paper, the transient behavior of two 230 kV CCVTs and one CT models are evaluated. The CCVTs are named as CCVT 1 and CCVT 2, and the required circuit topology and parameters are reported in [13], p. 42, and [14], p. 2 and 8, respectively. The CT parameters are described in [13], p. 41.

The CCVT 1, CCVT 2, and CT frequency responses are shown in Figs. 2, 3, and 4, respectively, which were obtained using the ATP Frequency Scan routine [7]. The frequency response of the conjunction of IT and anti-aliasing filters are also shown in the same figures. The frequency responses are plotted considering primary signals (K_{pri}), secondary signals (K_s), secondary and second order Butterworth filters with $f_c = 9$ kHz (K_{sB2}) and $f_c = 180$ Hz (K_{s180B2}), secondary and third order Butterworth filters with $f_c = 9$ kHz (K_{sB3}) and $f_c = 180$ Hz (K_{s180B3}), and secondary and third order Chebyshev filters with $f_c = 9$ kHz (K_{sC3}) and $f_c = 180$ Hz (K_{s180C3}), where K is V for voltage or I for current waveforms. The primary and secondary signals were normalized in per unit values in order to make possible some comparative analysis. The angle responses are presented in degrees. Despite the CCVT 2 shows an unusual magnitude frequency response (see Fig. 3(a)), all of its parameters were obtained from laboratory measurements [14].

At fundamental frequency, the IT present acceptable accuracy once the secondary voltages and currents are quite similar to the respective primary waveforms (see Figs. 2, 3, and 4), even when the anti-filters are taken into account. However, when the power network goes through a transient state, the secondary voltages differs from the primary signals in such a way that off-nominal frequency components are amplified or attenuated depending on the CCVTs frequency responses, which can affect high frequency measurements accuracy and protective relaying algorithms' performances. Regarding to the CT transient behavior, a typical CT model presents a magnitude frequency response constant over a wide frequency range (up to 50 kHz). For practical purposes, the CT may be regarded as having no impact on the spectral content of the input current signal, under conditions of the ferromagnetic core is not saturated [2]. On the other hand, when the anti-aliasing filters are considered, the secondary currents may be distorted in relation to the respective primary current (see Fig. 4).

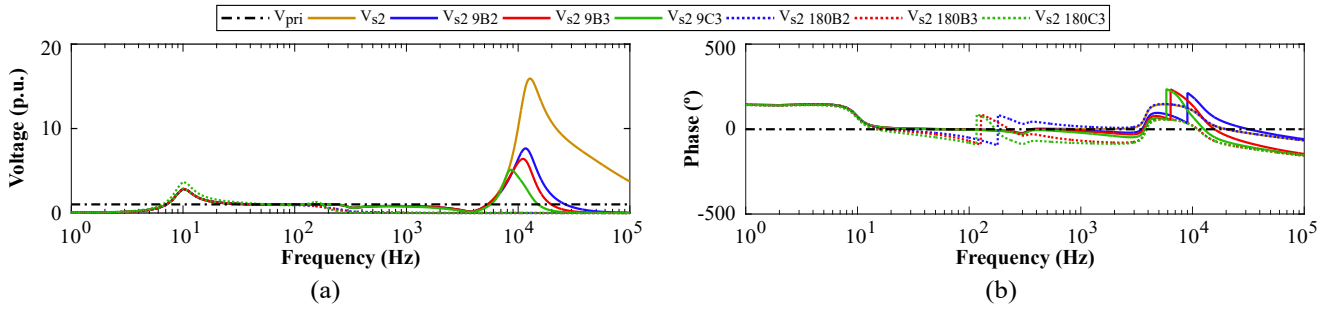


Fig. 3. CCVT 2 frequency response: (a) magnitude (p.u.); (b) phase ($^{\circ}$).

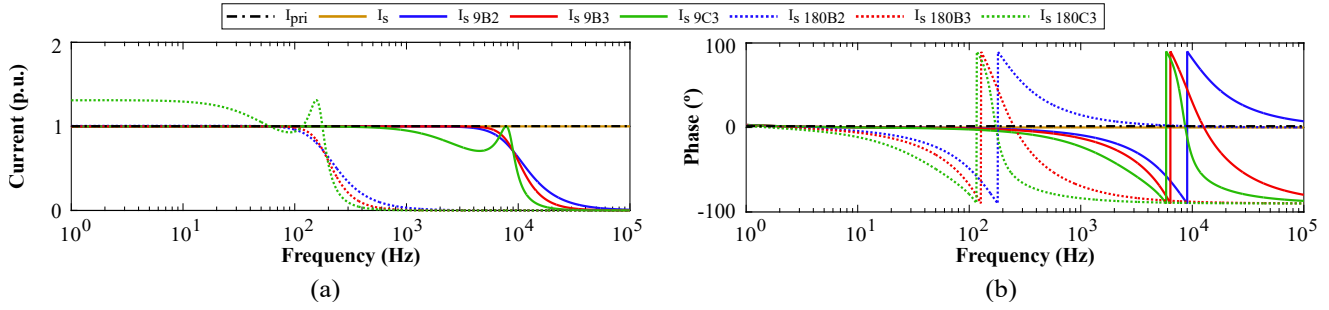


Fig. 4. CT frequency response: (a) magnitude (p.u.); (b) phase ($^{\circ}$).

The dynamic behavior of each analyzed IT in time domain is shown in Fig. 5 for a single line to ground fault located at 25 km away from the monitored bus on a 230 kV electric power system, which is described in section IV.

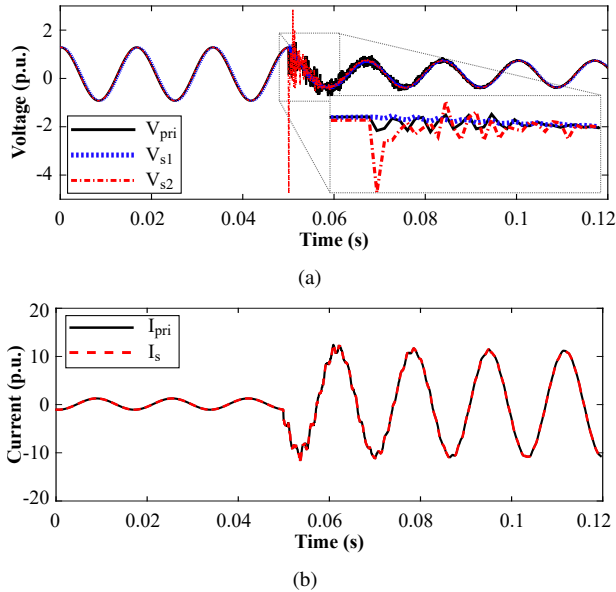


Fig. 5. Secondary waveforms due to a single line to ground fault: (a) voltage; (b) current.

From Fig. 5(a), it is noticeable that CCVT 1 and CCVT 2 secondary voltages (V_{s1} and V_{s2} , respectively) do not adequately follow the primary voltage waveform (V_{pri}) after the fault inception. V_{s2} significantly amplifies the high frequency components, according to its frequency response (see Fig. 3(a)). On the other hand, V_{s1} presents considerable attenuations on the off-nominal frequencies (see Fig. 2(a)). In both V_{s1} and V_{s2} , some phase displacements in relation to V_{pri} are presented as

well. In the case of current measurements depicted in Fig. 5(b), since the electromagnetic flux in the CT core is operating in the linear region, the secondary current signal (I_s) is almost an ideal replica of the primary current (I_{pri}). In this way, the IT transient behavior may affect the secondary measurements and transfer undesired information to fault locators.

IV. ANALYSIS AND RESULTS

Several ATP fault simulations were performed in the power network shown in Fig. 6, which is based on the one proposed in [13] for protection studies, in order to evaluate the impact of the analyzed IT and anti-filters on the fault locators. All the short-circuits were applied in TL 3. The line length of each TL is 150 km. The ATP time step was chosen as $2 \mu s$.

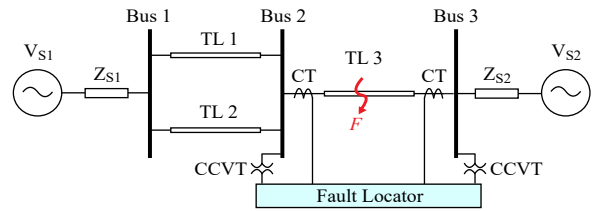


Fig. 6. 230 kV electric power system used in ATP simulations.

After each simulation, the fault point is estimated considering as input signals to the fault location algorithms the primary signals, secondary waveforms, and filtered secondary signals. Here, the primary signals are taken as reference. In the cases of travelling wave-based evaluations, the fault distance is estimated considering only voltage samples as input data, only current samples as input, and both voltage and current samples simultaneously. In situations that voltage and current samples are available concomitantly, the first fault-induced transient is detected in relation to the first incident wave reaching the monitored TL bus, whether it is voltage or current.

A total amount of 1050 fault scenarios were performed for each analyzed signal¹. In each simulation, the fault inception angle, fault resistance, fault type, and fault location were varied. The simulation variables are shown in Table I.

TABLE I
SIMULATION VARIABLES USED IN EACH FAULT SITUATION

Simulation variables	Values
Fault location (km)	25, 50, 75, 100, 125
Fault type	AG, BG, CG, AB, BC, CA, ABG, BCG, CAG, ABC
Inception angle (°)	0, 30, 60, 90, 120, 150, 180
Fault resistance (Ω)	0.1, 1, 7

The fault location relative error ϵ_k is computed as:

$$\epsilon_k(\%) = \frac{|d - \tilde{d}_k|}{\ell} \cdot 100, \quad (10)$$

where d is the actual fault location, \tilde{d}_k is the estimated fault distance, ℓ is the TL length, and k is the input signal (primary, secondary, or filtered secondary samples). Considering that f_s is 50 kHz and v was taken in this paper as 98% of the speed of light in free space, the maximum admissible error is 5.88 km ($\Delta t \cdot v$), which is approximately 3.9% of the TL length. Since ϵ_k is computed after each simulation, an error function is generated from the total amount of fault cases, whose obtained average values μ_ϵ and standard deviations σ_ϵ are shown in Table II for the travelling wave-based techniques.

TABLE II
INFLUENCE OF IT ON TRAVELLING WAVE-BASED FAULT LOCATORS

Relative errors (%)	Monitored signals*	Analyzed IT				
		CCVT 1	CCVT 2	CT	CCVT 1 & CT	CCVT 2 & CT
μ_ϵ	K_{pri}	0.498	0.498	0.495	0.498	0.498
	K_s	0.519	0.485	0.492	0.492	0.498
	K_s 9B2	0.649	0.476	0.501	0.502	0.471
	K_s 9B3	0.536	0.532	0.548	0.532	0.492
	K_s 9C3	0.677	0.570	0.684	0.677	0.575
σ_ϵ	K_{pri}	0.567	0.566	0.564	0.566	0.566
	K_s	0.571	0.557	0.562	0.561	0.566
	K_s 9B2	0.586	0.545	0.552	0.551	0.540
	K_s 9B3	0.594	0.593	0.603	0.592	0.560
	K_s 9C3	0.679	0.599	0.683	0.678	0.601

* K is the V or I samples, depending on the analyzed IT. In cases which both V and I samples are simultaneously available, as in CCVT 1 & CT and CCVT 2 & CT, K means V and I .

To investigate in more detail the travelling wave-based fault locator's performance, the percentage errors are presented as boxplots in Fig. 7, which are plots able to visually reveal some basic statistics of a data set, using five thresholds: the maximum value, represented by the upper whisker; the upper quartile, represented by the upper boundary of the box; the median quartile, represented by the intermediate line inside

¹1050 fault simulations when V_{pri} is taken as input data for the travelling wave-based fault locator, 1050 fault simulations when V_{pri} and I_{pri} are taken as input data for the impedance-based techniques, etc.

the box; the lower quartile, represented by the lower boundary of the box; and the minimum value, represented by the lower whisker. The upper quartile, the median and the lower quartile represent the maximum fault location error in 75%, 50% and 25% of the simulated fault cases, respectively.

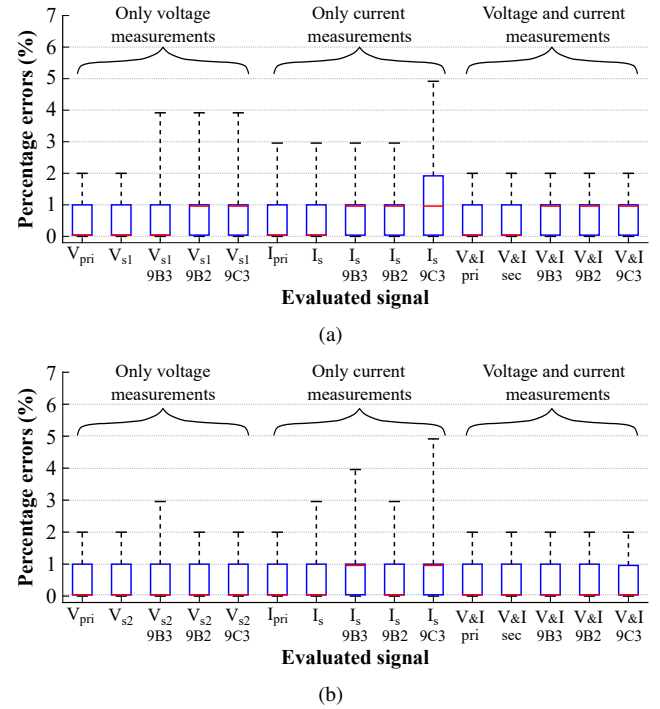


Fig. 7. Boxplots representing the travelling wave-based fault location percentage errors: (a) CCVT 1 and CT; (b) CCVT 2 and CT.

From the results presented in Table II and in Fig. 7, when only voltage measurements are available at the monitored buses, the μ_ϵ and σ_ϵ results are higher for the CCVT 1 secondary and filtered secondary samples than the ones obtained with the reference signal (V_{pri}). In fact, CCVT 1 frequency response significantly attenuates high frequencies (see Fig. 2(a)), which affects the fault-induced transient detection processes since they are more sensitive to the highest frequency spectrum. On the other hand, the μ_ϵ and σ_ϵ are smaller than the ones computed by V_{pri} when the CCVT 2 secondary and filtered secondary waveforms are taken as input data. In these scenarios, the travelling wave-based fault locator's performance was improved once CCVT 2 transient behavior amplifies high frequencies (see Fig. 3(a)), which makes the fault-induced transient detection procedure easier. When only current measurements are available, the fault distances are estimated more accurate than when the CCVT 1 secondary voltages were considered as input data. However, the best results were obtained when voltage and current signals are available simultaneously. In these cases, the maximum errors were smaller than when only voltage or current measurements were available, irrespective to the analyzed CCVT (see Fig. 7), indicating that the travelling wave-based fault locator's performance is more accurate and reliable. Regarding the solutions computed with the filtered secondary signals, the second order Butterworth filter has shown to be more appropriate to be used in cascade with the IT analog signals. The third order Chebyshev filter has shown the poorest results, which may be

due to the oscillations presented in the bandpass (see Fig. 1(a)). In addition to it, the maximum admissible error was only exceeded with the use of this filter in cascade with secondary current signals (see Fig. 7). It should be pointed out that smaller errors would be achieved for higher sampling rates. However, irrespective to the sampling rate used, the CCVT secondary voltage may be quite different from the primary voltage during faults (see Fig. 5(a)). In such cases, information not found at the primary side can be transferred to the fault locators as input data, affecting the fault locators' performance.

The obtained μ_ϵ and σ_ϵ for the impedance-based algorithms are shown in Table III.

TABLE III
INFLUENCE OF IT ON IMPEDANCE-BASED FAULT LOCATORS

Analyzed IT	Monitored signals*	One-ended Method		Two-ended Method	
		μ_ϵ	σ_ϵ	μ_ϵ	σ_ϵ
CCVT 1 & CT	K_{pri}	1.072	1.316	0.250	0.221
	K_s	1.084	1.413	0.414	0.386
	K_s 180B2	0.782	1.394	0.421	0.383
	K_s 180B3	0.782	1.393	0.421	0.383
	K_s 180C3	0.831	1.395	0.455	0.412
CCVT 2 & CT	K_{pri}	1.076	1.325	0.219	0.185
	K_s	1.085	1.326	0.585	0.680
	K_s 180B2	0.503	1.054	0.146	0.100
	K_s 180B3	0.493	1.053	0.146	0.100
	K_s 180C3	0.525	1.067	0.165	0.125

* K means V and I samples, depending on the analyzed IT.

From the results shown in Table III, the best solutions were obtained by the two-ended method, as was expected since two-terminal techniques use more input data to estimate the fault point. The μ_ϵ and σ_ϵ for both one- and two-terminal algorithms were higher than the ones obtained with the reference signals when the secondary waveforms were considered. Particularly to the CCVT 2 and CT results, the μ_ϵ and σ_ϵ were higher than the ones obtained with CCVT 1 and CT. In fact, the high frequency components amplified by the CCVT 2 transient behavior (see Fig. 3(a)) affect the phasor estimation procedure, which in turn compromise the fault location performance. Considering the filtered secondary samples as input data, the second and third order Butterworth filters have shown to be more suitable to be used in conjunction with the IT outputs, with the third order Butterworth filter showing slightly better results. In general, the results obtained with the usage of anti-aliasing filters were better since frequency components higher than f_c are attenuated, which improves the phasor estimation performance and, consequently, the fault location procedure. The worst solutions were provided by the Chebyshev filter, probably due to the oscillations at the bandpass (see Fig. 1(a)).

V. CONCLUSION

The impact of two CCVT and one CT in cascade with three different analog low-pass anti-aliasing filters on a two-ended travelling wave-based and one- and two-terminal impedance-based fault techniques were investigated. Several ATP fault simulations were performed varying fault parameters as resistance, inception angle, location, and type. In each simulation,

the fault point was estimated using the primary, secondary, and filtered secondary signals as input to the fault locators.

From the obtained results, the travelling wave-based performance was more affected when CCVT transient behavior attenuates high frequency components, since this technique is more sensitive to higher frequencies. In cases in which the CCVT amplifies high frequencies, the performance was improved. However, the best solutions were found when both voltage and current samples were available simultaneously. Regarding the anti-aliasing filters, the second order Butterworth filter has shown to be more appropriate for travelling wave-based applications.

In relation to the impedance-based routines, the two-ended method has shown to be more immune to the IT transient behavior. However, the poorest results were found when the CCVT amplifies high frequencies, which may affect the phasor estimation procedure, and, consequently, the fault locator's performance. The use of anti-aliasing filters provided better results once frequency components higher than the cut-off frequency are attenuated, which improves the phasor estimation the fault location performances. In both travelling wave-based and impedance-based analysis, the highest errors were computed when the Chebyshev filter were used.

REFERENCES

- [1] M. M. Saha, J. Izykowski, and E. Rosolowski, *Fault Location on Power Networks*, ser. Power Systems. London: Ed. Springer, 2010.
- [2] B. Naodovic, "Influence of instrument transformers on power system protection," Ph.D. dissertation, Texas A&M University, 2005.
- [3] A. G. Phadke and J. S. Thorp, *Computer Relaying for Power Systems*, 2nd ed., ser. Protective relays. England: A John Wiley and Sons Ltd, 2009.
- [4] R. L. A. Reis, F. V. Lopes, W. L. A. Neves, and D. F. Jr., "Influence of coupling capacitor voltage transformers on travelling wave-based fault locators," *International Conference on Power Systems Transients*, June 2015.
- [5] D. Hou and J. Roberts, "Capacitive voltage transformer: transient overreach concerns and solutions for distance relaying," in *Electrical and Computer Engineering, 1996. Canadian Conference on*, vol. 1, May 1996, pp. 119–125 vol.1.
- [6] F. B. Costa, "Fault-induced transient detection based on real-time analysis of the wavelet coefficient energy," *IEEE Transactions on Power Delivery*, vol. 29, no. 1, pp. 140–153, Feb 2014.
- [7] *ATP - Alternative Transient Program*, Leuven EMTP Center, Herverlee, Belgium, 1987.
- [8] P. F. Gale, P. A. Crossley, X. Bingyin, G. Yaozhong, B. J. Cory, and J. R. G. Barker, "Fault location based on travelling waves," in *Developments in Power System Protection, 1993., Fifth International Conference on*, 1993, pp. 54–59.
- [9] S. L. Zimath, M. A. F. Ramos, and J. E. S. Filho, "Comparison of impedance and travelling wave fault location using real faults," in *IEEE PES T D 2010*, April 2010, pp. 1–5.
- [10] S. Das, S. Santoso, A. Gaikwad, and M. Patel, "Impedance-based fault location in transmission networks: theory and application," *IEEE Access*, vol. 2, pp. 537–557, 2014.
- [11] T. Takagi, Y. Yamakoshi, M. Yamaura, R. Kondow, and T. Matsushima, "Development of a new type fault locator using the one-terminal voltage and current data," *IEEE Transactions on Power Apparatus and Systems*, vol. PAS-101, no. 8, pp. 2892–2898, aug. 1982.
- [12] G. Benmouyal, "Removal of dc-offset in current waveforms using digital mimic filtering," *IEEE Transactions on Power Delivery*, vol. 10, no. 2, pp. 621–630, Apr 1995.
- [13] *EMTP Reference Models for Transmission Line Relay Testing*, IEEE Power System Relaying Committee, 2004. [Online]. Available: <http://www.pes-psrc.org>
- [14] A. V. Carvalho, A. R. F. Freire, and H. M. de Oliveira, "Transient interaction between coupling capacitors voltage transformers and transmission lines," in *2009 IEEE Power Energy Society General Meeting*, July 2009, pp. 1–8.